Hindawi
Advances in Mathematical Physics
Volume 2018, Article ID 5462659, 11 pages
https://doi.org/10.1155/2018/5462659

Research Article

A New Approach to Determine Gas Diffusion Coefficients in Porous Solids by EIS: Application for NH_3 and CO_2 Adsorption on Zirconia and Zeolite Type 5A

Tien-Quang Nguyen, Maja Glorius, and Cornelia Breitkopf

Chair of Technical Thermodynamics, Faculty of Mechanical Science and Engineering, Technical University of Dresden, Helmholtzstr. 14, Dresden 01069, Germany

Correspondence should be addressed to Tien-Quang Nguyen; quang_nguyentien2001@yahoo.com and Cornelia Breitkopf; cornelia.breitkopf@tu-dresden.de

Received 6 July 2018; Revised 12 September 2018; Accepted 18 September 2018; Published 4 October 2018

Academic Editor: Ivan Giorgio

A new theoretical approach has been established to define transport coefficients of charge and mass transport in porous materials directly from impedance data; thus four transport coefficients could be determined. In case of ammonia adsorption on sulfated zirconia, the diffusion coefficient was figured out to be approximately the mobility diffusion coefficient of ammonium ions: 1.2 x 10^{-7} cm^2/s. The transport of carbon dioxide was examined for samples of zeolite type 5A in different hydration states. By impedance spectroscopy measurements, the diffusion coefficient of water vapor at 373 K is estimated to be about 7 x 10^{-6} cm^2/s. The influence of carbon dioxide adsorption on diffusion coefficients is studied based on two pellet types of zeolite 5A. The difference between polar and non-polar gas adsorption in porous solids is considered as changed characteristic of impedance.

1. Introduction

Gas transport in porous material plays a significant role in industrial applications, especially in electrocatalysis, batteries, and gas sensor research. Zeolites and zirconias are ionic conducting materials used as gas sensor [1–6] at high temperatures and are proton conducting at low temperatures [7]. Diffusion of gases in these catalysts has been published, i.e., in zeolite [5, 6, 8, 9] and in sulfated zirconia [1, 3, 10, 11]. However, it has not been measured by EIS so far.

Electrochemical impedance spectroscopy (EIS) has proven to be a powerful tool to investigate mass and charge transfer processes [3, 6, 12, 13]. The gas phase adsorption on porous solid has been studied by impedance spectroscopy of pure gases regarding the change of capacitance [14], electrical conductivity [5, 6, 10], and impedance at low frequencies depending on gas concentration [4]. In the meantime, many models of gas phase diffusion have been built by using EIS for fuel cells such as the stagnant gas layer above electrodes [1, 3], gas diffusion electrodes [15], and mass transport contribution in diffusion limitation [12].

Ammonia is a well-known probe gas to investigate acid property of porous catalysts thanks to the high selectivity of small molecules. Accordingly, various types of ammonia sensor have been developed from sensing materials like proton conductor, semiconductor, and polymers. Recently, Satsuma and coworkers [10] have reported a good response of ammonia sensing on thick film tungstated-zirconia. They indicated from results of impedance spectroscopy method that ammonia plays a significant role in increasing the conductivity of tungstated-zirconia. Previously, this had been pointed out in case of NH_3 adsorption on zeolites [5, 6]. They suggested the sensing mechanism of proton diffusion by hopping in zeolites, which was then modified by Satsuma [10] that surface adsorbed species such as ammonia play a part in the solvation-supported proton transport. However, there has not been any evaluation of ammonia diffusion in sensing porous materials despite its important effect on the performance of sensors. Therefore, ammonia diffusivity is very worth concerning as diffusion process takes place slowly in porous materials. Transport coefficients of ammonia in different porous media have been reported in numerous

experimental methods, i.e., the isothermal transient ionic current method [16], NMR [17, 18], and vacuum-TPD [13, 19]. So far, it has not been measured by EIS method.

Carbon dioxide through zeolite type A is an interesting issue due to their selective cation exchangers in numerous applications, such as air separation and gas separation of CO_2 from waste gas emissions [2, 20, 21]. Investigation of this diffusion phenomenon seems to be restricted regarding the number of experimental methods. The diffusion coefficient of CO_2 on zeolite 5A has been measured by NMR [8], frequency response [22], gas chromatography [23], and gravimetric method [9].

In principle, the transport diffusion for mass in impedance spectroscopy method is described by Fick's law which lays the foundation for the Warburg impedance [24]. In addition, the diffusion coefficient of mobile charge is also defined by impedance spectroscopy based on the Nernst-Einstein relation [25]. In comparison with other experimental methods, with respect to the diffusivity of proton/water in FAU-type zeolite [26], the diffusivities are measured by quasi-elastic-neutron (QENS) based on the concentration of water molecules in zeolite. Meanwhile, the diffusivities of CO_2 in zeolite (including LTA) were found to follow Arrhenius law [27].

In this study, transport coefficients of gas phases in porous pellets are obtained by means of impedance spectroscopy. These parameters are calculated directly from experimental data based on available models in literature and new proposed approaches in case of gas phase effect. Diffusion coefficients are determined by separate calculations of net ionic mobility and gas phases. IR spectroscopy data are combined in analyses with respect to mechanism and position of gases on the surface of porous catalysts.

2. Experimental

2.1. Material. Sulfated zirconia (SZ) based on zirconium hydroxide XZO 1720 with 10 wt.-% SO_3 from MEL Chemicals is used to study the transport of ammonia. Zeolite type 5A provided by Chemiewerk Bad Köstritz GmbH (Germany) as molecular sieve Köstrolith® 5AK/ABFK is applied for carbon dioxide adsorption and transport. Powder is sieved with grain diameters smaller than 0.1 μm before they are utilized for the experiments.

2.2. Preparation and Pretreatment Sample

2.2.1. Sulfated Zirconia Pellets. The MEL precursor was calcined at 873 K for 3 h in air flow of 0.03 NL/min. After being cooled to room temperature, about 150 mg of the dried powder was pressed (3 Ton) into a pellet with a diameter of 13 mm. The pellet was then contacted with silver paste (by Sigma Aldrich) on both faces. After that, the sample was placed into the EIS-chamber and heated at 383 K for 2 h in ambient atmosphere before the measurement. The thickness of the sample is 0.8 mm.

2.2.2. Zeolite 5A Pellets. Zeolite type 5A was pressed (4 Ton) into a pellet with a diameter of 13 mm. Two types of pellets with different thicknesses (0.65 mm and 0.35 mm) have been prepared. The pellets were contacted with silver paste (by Sigma Aldrich) on both faces and the silver layer had been dried at room temperature before the next thermal treatment was carried out.

For the first sample with thickness 0.65 mm (Z5A-1), they were heated at 573 K for 2 h in air flow of 0.03 NL/min and cooled to room temperature before being located into the cell chamber. The second sample (Z5A-2) was directly put into the closed chamber and heated at 473 K for 30 min. Then it was reduced to 373 K and held at this temperature until the first measurement in the closed chamber.

2.3. Impedance Measurement. The measurements by EIS were carried out before and after gas loading (i.e., NH_3 through sulfated zirconia and CO_2 through zeolite 5A) at the same temperature. In principle, the sample was maintained at the desired temperature for at least 30 min before the first measurement. The sample is kept between two copper surfaces which are connected to Autolab PGSTAT302N (Eco-Chemie, Netherlands). Electrochemical impedance measurements were conducted by two electrodes without reference electrode in a frequency range from 0.01 Hz to 100 kHz. The silver paste is used to improve electrode/electrolyte contact. The influence of the silver paste layer can be ignored at low temperatures. Electrical linearity of the sample response has been examined in a voltage amplitude range of 10-250 mV. In order to obtain the best current resolution, a measuring voltage of 250 mV is chosen so that the responses are found to be linear, which obeys Ohm's law. The impedance data are analyzed by fitting with equivalents circuit by NOVA integrated into Autolab PGSTAT 302N.

3. New Theoretical Approach to Evaluate Transport Parameters

3.1. Diffusion Coefficients of Mobile Species. A model of ionic concentration polarization between two blocking electrodes is applied for the macroscopic space-charge polarization by Coelho [28]. The equivalent circuit of this model includes RC parallel for electrolyte series doulbe-layer capaciatance and C_{dl} for interface of electrode/electrolyte. In non-Debye relaxation, capacitance elements will be replaced by constant phase element (CPE). From the analysis of the effective complex permittivity, Bandara and Mellander [25] suggested the diffusion coefficient of ionic mobile species as the following:

$$D_m = \frac{\lambda_D^2}{\tau_2}, \tag{1}$$

where τ_2 is the characteristic time constant which corresponds to the peak point on the loss tangent (Figures 1(a) and 1(b)). Parameters at the peak are given as

$$\tan(\phi)_{max} = \frac{\sqrt{\delta}}{2} \tag{2}$$

at $\tau_2 = \tau_1 \sqrt{\delta}$

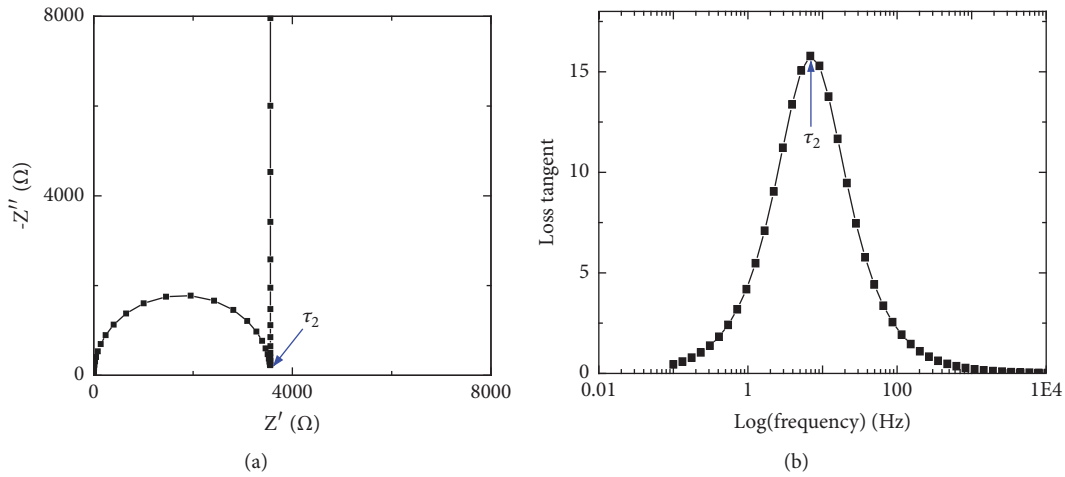

Figure 1: (a) Nyquist and (b) loss tangent plots for a general equivalent circuit of a sample in between two blocking electrodes.

The Debye length λ_D is calculated as the ratio of a sample thickness, d with the dimension-less, δ:

$$\lambda_D = \frac{d/2}{\delta} = \frac{d/2}{(2 \cdot \tan(\phi)_{max})^2} \quad (3)$$

This model assumes that the dimensionless $\delta >> 1$. According to Coelho [28], the good approximation is typically applied for $\delta \geq 10$.

3.2. Chemical Diffusion Coefficient. This value originates from the fitting of a finite-length Warburg element with impedance data at low frequencies.

$$Z_{W-O} = \frac{R_D}{\sqrt{j\omega\tau_D}} \tanh\left(\sqrt{j\omega\tau_D}\right) \quad (4)$$

with j being imaginary unit

In this paper, the Warburg impedance is separated into the real and imaginary part. Diffusion parameters, i.e., R_D and τ_D, are obtained by fitting imaginary data with the imaginary part of the Warburg element. The results will refer to the fitting outcome of programs such as NOVA, Zview from corresponding equivalent circuits. In fact, the fitting value by an equivalent circuit is likely to have a significant deviation in the appearance of Warburg element due to the number of noisy points by mass transport at low frequencies. Then, the chemical diffusion coefficient is defined as an equation,

$$\widetilde{D} = \frac{l_D^2}{\tau_D}, \quad (5)$$

if the diffusion length l_D is known. Under the condition of incomplete diffusion limitation, this diffusion coefficient has a significant contribution from mass transport [12]. By that means, the diffusion length is bigger than the Debye length, which is computed based on the assumption of the electron lifetime [29] and equals the summit frequency.

$$l_D = \sqrt{D_m \cdot \tau_{life-time}} \quad (6)$$

3.3. Effective Diffusion Coefficient D_e. The effective diffusion coefficient is estimated by (7) via the stagnant gas layer model [3],

$$D_e = \frac{l_{st}^2}{\tau_D}, \quad (7)$$

where τ_D is the diffusion time constant and l_{st} is the thickness of the stagnant gas layer.

In electrochemical systems, the diffusion coefficient of the bulk gas in a stagnant gas layer above the electrode surface relates to the effective diffusion coefficient which is described by the finite-length Warburg component [1, 3, 12]. Most electrochemical systems have this diffusivity which is caused by the mass exchange between a species source or the sink location and surface electrodes [1]. The stagnant gas layer is calculated based on the summit frequency, f_s, that is the maximum frequency of a pseudo-RC parallel circuit. This circuit replaces the finite-length Warburg element because of increasing capacitance of the double-layer by gas phase diffusion and the binary diffusion coefficient. It is computed as (8) [3]:

$$l_{st} = \sqrt{\frac{2.53 \cdot D_{12}}{2\pi f_s}} \quad (8)$$

In (8), the binary diffusion coefficient D_{12} is determined by the Chapman-Enskog model:

$$D_{12} = 1.883 \cdot 10^{-22} \frac{T^{3/2}}{p\sigma_{12}^2 \Omega_D} \sqrt{\frac{1}{M_1} + \frac{1}{M_2}}, \quad (9)$$

where T is absolute temperature in Kelvin, p is pressure in Pascal, M is molar weight of the gases, and σ_{12} and Ω_D are parameters of gases calculation from Lennard-Jones potentials.

3.4. Diffusion Coefficient by Jumping between Two Neighboring Sites. In some cases of solid materials such as zeolites,

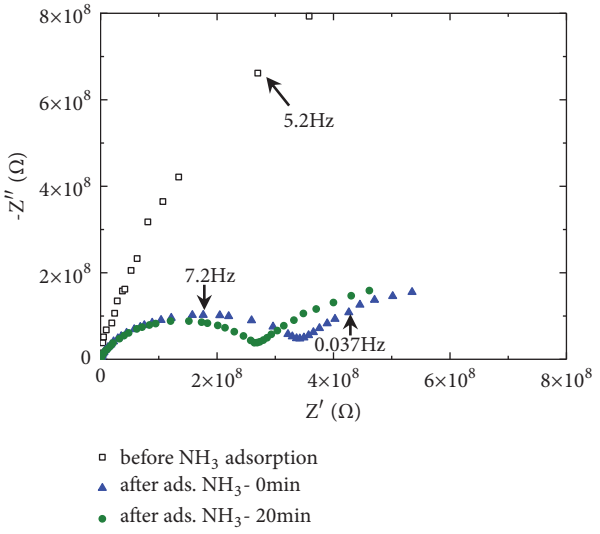

FIGURE 2: Nyquist plot of sulfated zirconia before and after loading ammonia at 383 K.

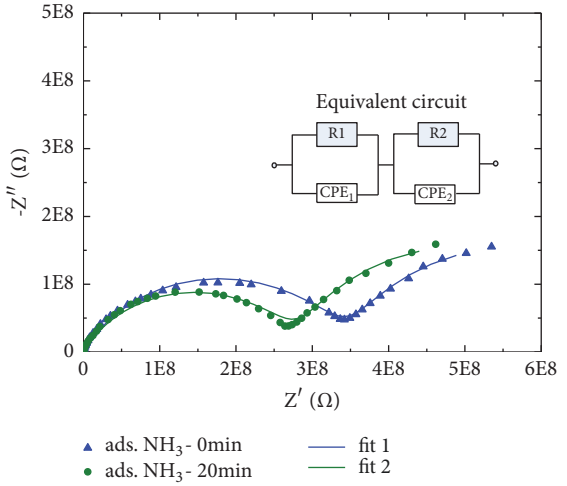

FIGURE 3: Fit of experimental data by the equivalent circuit with respect to Figure 2.

the capacitance of the pellet reaches high values at low temperatures. As a result, the loss tangent at the peak is small due to the high value of Z''. In these cases, the dimensionless δ is smaller than 10 and the Bandara-Mellander model cannot be employed. The average distance jump of mobility by the hopping model will replace the Debye-length in (1). Hence, the diffusion coefficient by jumping is explained by

$$\overline{D} = \frac{\Gamma^2}{\tau_2}, \tag{10}$$

where τ_2 is the time constant at the peak on the loss tangent. The characteristic time constant is minimal (10^{-3} - 10^{-5} s). At that time, the average distance jump can be followed by the model of Rolling et al. [30] and Dygas [31].

The square of the average distance jump is defined by

$$\Gamma^2 = \frac{\varepsilon_o \Delta\varepsilon}{\sigma}\omega_O = \frac{1}{P}\frac{\omega_O}{\omega_C} \tag{11}$$

where ω_O, ω_O, ε_o, and σ_o are onset frequency, relaxation frequency, permittivity of vacuum, and dc conductivity, respectively. The parameter Γ is interpreted as an average length or element jump distance of relative charge shift, caused by local rearrangements of hopping carriers [31]. The dimensionless P or the Barton-Nakajima-Namikawa relation provides valuable information about unit jump length and units of average time between jumps of a hopping carrier [31].

4. Results and Discussion

4.1. Ammonia on Sulfated Zirconia

4.1.1. Influence of Ammonia Adsorption on Impedance. Figure 2 shows the Nyquist plots for sulfated zirconia samples before and after ammonia is loaded. It includes a semicircle at high frequencies and a tail at low frequencies. The semicircle is characterized by the grain and grain boundary geometry. The profiles of impedance spectra indicate that the characterization of the grain or grain boundary can be interpreted in terms of a RC parallel equivalent circuit. In solid electrochemistry, the surface roughness is one of the factors which has a significant contribution to frequency dispersion. Such behavior is generally analyzed by replacing a capacitor by a constant phase element (CPE) [32]. At low frequencies, the appearance of a tail is attributed to gas phase diffusion in diffusion limitation condition. From EIS point of views, the low-frequency dispersion is interpreted in terms of the Warburg impedance by a diffusion process [33]. On the contrary, owing to the contribution of bulk gas diffusion, the double-layer capacitance increases. As a consequence, the spectra at low frequencies will form a semicircle fitted by R-CPE parallel, which is proposed by the studies in [3, 12]. The equivalent circuit and fitted curves are illustrated in Figure 3.

The semicircle decreases significantly after ammonia adsorption (Figure 2), which implies that the electrical conductivity of the sample increases. The ionic conductivity is described by the number of ions present and their respective mobility was ascribed for adsorbed NH_4^+ -ions [5, 6, 10]. Fundamentally, ammonia molecules act on Brønsted acid sites at the surface of sulfated zirconia via H-bonding. Protons from OH-groups will transfer to ammonia molecules to generate ammonium ions. During that time, ammonia acts as a solvation-supported proton transport, which is similar to the Grotthuss mechanism. The dependence of proton diffusion on the temperature resembles the description in [34]. Therefore, the electrical conductivity σ depends on the mobility of migrating species μ and the concentration of NH_4^+ ions, as follows:

$$\sigma = F \cdot z \cdot \mu \cdot \left[NH_4^+\right] \tag{12}$$

where F and z are the Faraday constant and the number of charged species, respectively.

Table 1: Diffusion coefficient of ionic mobility and ammonia in SZ (d = 0.8 mm) at 383 K.

	0 min$^{(*)}$	20 min
λ_D [μm]	1.948	2.040
l_D [μm]	11.8	15.6
τ_D [s]	14.8	16.6
$\mathbf{D_m}$ [cm^2/s]	**8.9 x 10^{-8}**	**1.4 x 10^{-7}**
$\widetilde{\mathbf{D}}$ [cm^2/s]	**9.4 x 10^{-8}**	**1.5 x 10^{-7}**

(∗): 0 min, starting measurement with EIS after 15 min loading in ammonia.

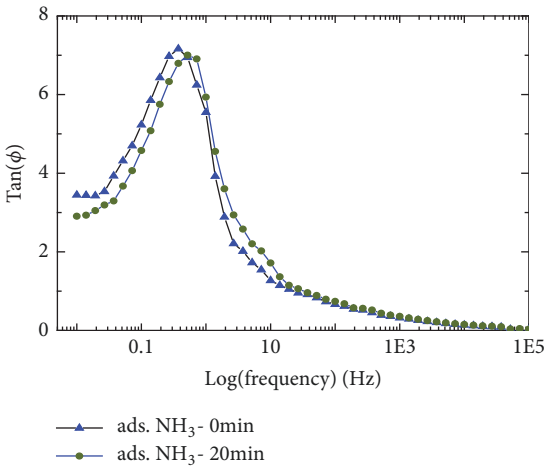

Figure 4: Loss tangent plot for ammonia adsorption on sulfated zirconia at 383 K.

4.1.2. Diffusion Coefficients. The diffusion coefficient of mobile ions is calculated by the peak point on the loss tangent plot at low frequencies (see Figure 4 and Section 3.1). Meanwhile, the diffusion coefficient of ammonia is extracted from the finite-length Warburg (see (4)). In order to estimate the summit frequency, the equivalent circuit is extended to the broad frequency range from 0.001 Hz to 100 kHz. A summary of diffusion parameters of ammonia adsorption on sulfated zirconia is illustrated in Table 1.

The diffusion coefficient of mobility increases slightly in the 2nd measurement. It shows that the conductivity of the sample grows with the time. By that means, it is suggested that the adsorption of ammonia is still occurring at other OH-groups on the surface of sulfated zirconia. Similarly, the chemical diffusion coefficient which is assumed by fitting data with the finite-length Warburg element also rises after 20 min of adsorption. In fact, the chemical diffusion coefficient has contributed to the bulk gas and charged species concentration [12]. However, the average value of mobility and chemical diffusion coefficients are determined to be about 1.2 x 10^{-7} cm^2/s. Therefore, it is recommended that most of ammonia gas promotes the formation of ammonium ions on the surface of sulfated zirconia. As a result, the diffusion coefficient of ammonia in sulfated zirconia equals the chemical diffusion coefficient, $\widetilde{D}$ = (0.9 -1.5) x 10^{-7} cm^2/s.

About the diffusion mechanism of mobile species, this phenomenon can be interpreted by proton hopping mechanism suggested by Franke and Simon [5, 6]. Accordingly, the presence of adsorbed ammonia acts as solvation-supported proton transfer via the Grotthuss mechanism at low temperatures. In particular, the adsorption of ammonia on sulfated zirconia was observed with NH_4^+- ions on surface acidic OH groups, i.e., the Brønsted acid sites. In fact, the water has not been fully eliminated at measurement conditions at low temperatures. However, in the presence of ammonia, the electrostatic attraction between free water and negative charged lattices of OH-groups decreases significantly, which produces a new ammonium ion. This excess proton can be delivered to a new unoccupied site or another NH_3 molecule [5]. Consequently, the mobility of ionic charges increases, resulting in an enhanced conductivity which is mainly proportional to the concentration of NH_4^+ -ions. The diffusion coefficient of mobile charged species is primarily given by NH_4^+-ions motion.

In literature, similar data are reported for ammonium ion diffusion in a cylindrical pellet of $(NH_4)_4Fe(CN)_6{\cdot}1.5H_2O$ by Gawad and Bhat [16] using the isothermal transient ionic current method, D = 3.87 x 10^{-7} cm^2/s. Their discovered value lies in the same range as for the investigated sulfated zirconia in this research, because the identical phenomenon of $NH_4^+ - ion$ diffusion in a cylindrical pellet and the experimental method is also applied by electrochemical system. Moreover, the diffusion coefficient of ammonia in Table 1 can be compatible with the self-diffusion coefficient of ammonia in some porous solids: in silica from 300 to 500 K by QENS (2.5 x 10^{-6} to 2.0 x 10^{-5} cm^2/s) and by PFG NMR (3 x10^{-7} to 1.5 x10^{-6} cm^2/s) [18]; in H-ZSM5 in range from 1 x10^{-7} to 2 x10^{-5} cm^2/s [17]. Its value depends on the concentration of ammonia on the surface and ignores the hopping diffusion of proton transport in NH_3 phase via NH_4^+ in the channel.

The effective diffusion coefficient of mixed gases above electrodes illustrated in Table 2 was previously calculated by (7)-(9). The experimental system is assumed to contain three gas phases: ammonia, water, and helium at 2 bar pressure and 383 K. In this case, the lowest binary gas mixture is used to determine the stagnant gas layer as (8). Accordingly, the binary diffusion coefficient of NH_3/H_2O is defined as the lowest, and its value is $0.161 cm^2/s$ based on the Lennard-Jones characteristic lengths in [35]. It can be seen that the effective diffusion coefficient during measurement is nearly constant. Their values are higher than the lowest binary

Table 2: Effective diffusion coefficients of mixed gas in the cell system at 383 K.

	0 min	20 min
Stagnant gas layer l_{st} [cm]	2.52	2.71
D_e [cm^2/s]	0.430	0.440

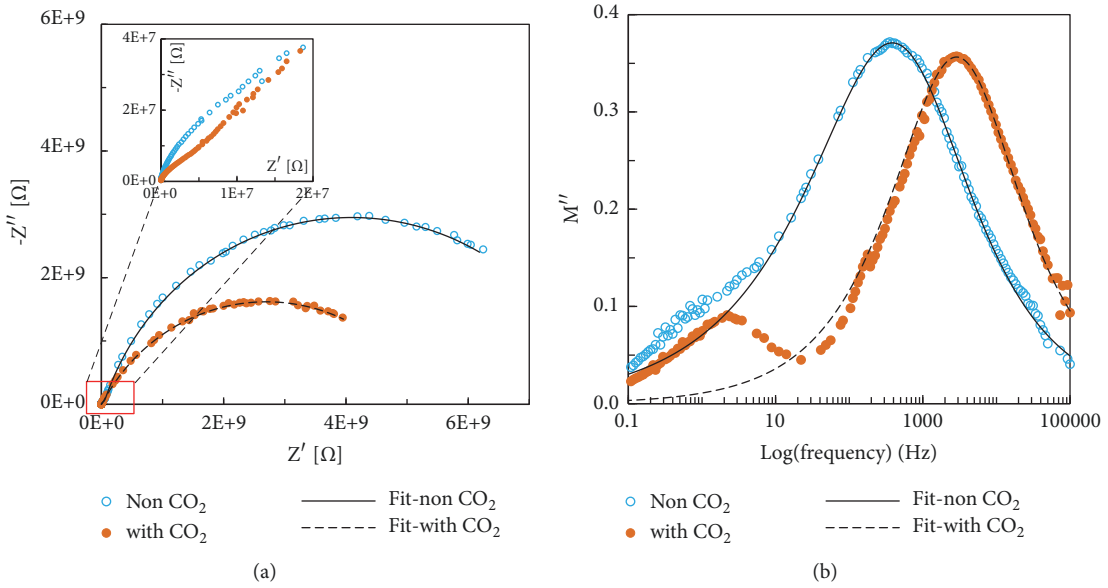

Figure 5: (a) Nyquist plot and (b) modulus loss M'' of Z5A-1 with and without loading CO_2 at 433 K.

diffusion coefficient nevertheless, which may be caused by Knudsen diffusion in pores [1]. Particularly, the increase of the stagnant gas layer can be explained by the decrease of ammonia concentration according to Nakajima [12]. In other words, ammonia gas above electrodes will continue to be adsorbed on the surface of sulfated zirconia.

4.2. Carbon Dioxide in Zeolite 5A. In order to obtain transport coefficients of carbon dioxide by means of EIS method, two different samples (Z5A-1 and Z5A-2) which correspond to high- and low-temperature treatment are investigated with adsorbed CO_2 gas.

4.2.1. Effect of CO_2 on Impedance at 433 K in Sample Z5A-1. Figure 5(a) displays the comparison of the impedance spectrum for zeolite Z5A-1 before and after carbon dioxide adsorption. It can be realized that the impedance of the sample decreases substantially after carbon dioxide is adsorbed. However, the impedance spectrum after carbon dioxide adsorption has been formed as similarly as in the absence of carbon dioxide. In specific, the impedance spectra of both cases consist of two semicircles which are attributed to the grain and grain boundary at high and low frequencies. The equivalent circuit includes two series of R-CPE parallel.

On the other hand, the relaxation distribution of ions on broad frequency ranges is more useful to display results as the modulus loss M'' (Figure 5(b)). It is extracted from the impedance by the expression

$$M'' = \omega C_o Z'. \tag{13}$$

Only one peak appears at medium frequencies before carbon dioxide is loaded, which suggests only single species relaxation. This maximum corresponds to the dipolar relaxation of Ca^{2+}- ion in α-cage since the activation energy of relaxation for this sample below 573 K is estimated to be about 86 kJ/mol (data from activation energy measurement of a similar sample). Besides, the simulated result by Demontis [36] showed that the activation energy ranging from 51 to 97 kJ/mol was not likely to enable cations Ca^{2+} and Na^+ jumping diffusion in zeolite 5A. Thus, the ion conduction can be assumed by protons. Actually, the proton presence on the surface of zeolite 5A can be observed by IR spectroscopy by two bridging OH-groups on super-cages (band at 3650 cm^{-1}) and sodalite-cages (band at 3512 cm^{-1}); see Figure 6. This result is in agreement with [20]. Moreover, a strong band at 3567 cm^{-1} is attributed to nonacid $[Ca(OH)]^+$ in the measurement temperature; this band is at 3555 cm^{-1} in [20]. The strong band appearance of $Ca(OH)^+$ in zeolite 5A can be interpreted by the hydroxylation of Ca^{2+} cations with even very small tracers of water [8]:

$$Ca^{++} + H_2O \longrightarrow [Ca\,(OH)]^+ + H^+ \tag{14}$$

This reaction takes place leading to the replacement of one divalent cation by two monovalent cations. In this case, proton motion is likely to happen between two neighboring cations.

After CO_2 adsorption, the impedance spectrum reduces significantly at low frequencies, which corresponds to an increasing conductivity; see Figure 7(a). The relaxation peak

Table 3: Parameters for calculation of CO_2 interaction on zeolite by Bandara-Mellander's model.

	f_m [Hz]	$\tan(\phi)$	δ
Before CO_2 ads.	242.93	0.479	0.917
After CO_2 ads.	838.16	0.531	1.128

Table 4: Diffusion parameters of proton mobility in Z5A-1 before and after adsorption carbon dioxide at 433 K.

	Γ^2[Å^2]	τ_2 [s]	$\overline{\mathbf{D}}$ (cm^2/s)
Before CO_2 ads.	1.065	$6.55.10^{-4}$	1.6 x10^{-13}
After CO_2 ads.	1.043	$1.90.10^{-4}$	5.5 x10^{-13}

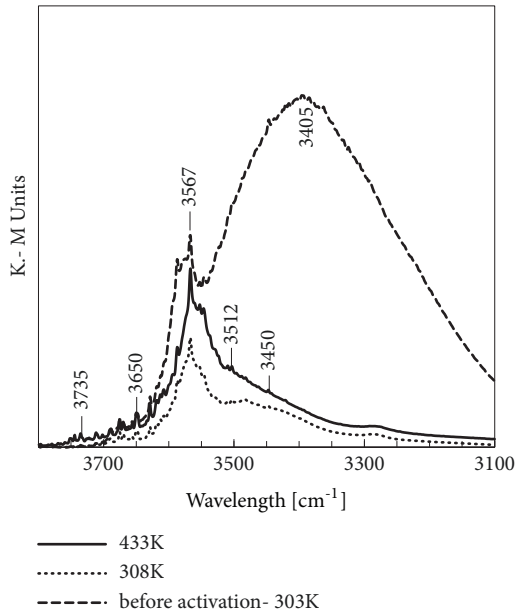

Figure 6: IR spectra for zeolite 5A before and after activation at 303 K and 433 K.

on the modulus M'' shifts towards higher frequencies, which implies that the conductivity relaxation mode of proton rises after CO_2 is loaded. Theoretically, the adsorption of carbon dioxide on zeolite can be modeled by the change of electric capacitance or electrical conductivity [4, 14, 37]. The growth of electrical capacitance as well as the dielectric constant after carbon dioxide had been adsorbed in a zeolite sample was supported by the theory of Kurzweil et al. [37] and Staudt et al. [14]. Accordingly, the raising capacitance of the capacitor causes an increase in the dielectric constant; see Figure 7(b).

The diffusion coefficients were first estimated via the Bandara-Mellander model based on the peak on the loss tangent plot (Figure 8). Regarding Table 3, the dimensionless δ is smaller than 10; hence the Bandara-Mellander model will not be employed in this case. The proton diffusion coefficient is calculated as in Section 3.3 in which the Debye length is replaced by the average length distance, Γ, as (11). Diffusion parameters of protons in Z5A-1 under the influence of carbon dioxide are defined in Table 4.

The proton diffusion coefficient increases slightly after carbon dioxide adsorption. From the viewpoint of the mechanism of CO_2 adsorption on zeolite 5A, it is assumed that this growth originates from the perturbation of carbon dioxide molecules to residual $[Ca(OH)]^+$ groups and cations Ca^{++} and Na^+ in order to generate OCO-Ca^{2+} and OCO-Na^+ ions. Furthermore, a minority of CO_2 adsorption on zeolite 5A is chemisorbed to form carbonate species because carbon dioxide does not interact with nonacidic OH groups on $Ca(OH)^+$ [20]. The interaction between carbon dioxide and acidic OH-groups only happens on zeolite protonic centers, i.e., Si-OH-Al bridging OH groups. Thus, the bonding of protons on oxygen atom becomes weak and the interaction of protons with neighboring sites rises more strongly than that. The minor growth of proton mobility diffusion coefficient reflects the perturbation but does not belong to the diffusion coefficient of carbon dioxide gas phase.

Theoretically, the proton mobility diffusion coefficients from OH groups are given from 10^{-13} to 10^{-11} cm^2/s in the temperature range 373 to 473 K in HNaY [38]. Similarly, Fripiat et al. [39] figured out the diffusion coefficients of proton jump in faujasite zeolite (X, Y) in temperature between 373 and 673 K about 3.4 x 10^{-14} to 3.1 x 10^{-9} cm^2/s with the jump distance of 4.4 Å. Therefore, the calculated value by EIS is appropriate to the proton diffusion coefficient.

4.2.2. Effect of CO_2 Diffusing in Sample Z5A-2. Figures 9(a) and 9(b) show impedance spectra and the fitted data curves of sample Z5A-2 before and after CO_2 loading. In both cases, the impedance can be analyzed with three semicircles. They are attributed to the grain at high frequencies, grain boundaries at intermediate frequencies, and interface at low frequencies (usually less than 10 Hz). The equivalent circuit model is fitted by an equivalent circuit with three series of R-CPE parallel (see Figure 9(b)). After CO_2 is loaded, the impedance increases primarily in the second and third arc at intermediate and low frequencies owing to the gas effect at low frequencies [4]. The impedance growth is caused by the reduction of the electrical conductivity. Therefore, there is no difference of impedance compositions for the sample with/without CO_2.

The electrical conductivity in the sample depends on the concentration of hydroxonium ions on the surface; see (12). In fact, the sample is heated in the closed chamber at low temperatures; the free water inside is desorbed to generate

Table 5: Diffusion coefficient of mobility and water vapor (cm^2/s) in Z5A-2 before and after CO_2 adsorption at 373 K.

	Before	After
$\mathbf{D_m}$	**5.9×10^{-5}**	**3.3×10^{-5}**
$\widetilde{\mathbf{D}}$	**8.3×10^{-6}**	**5.9×10^{-6}**

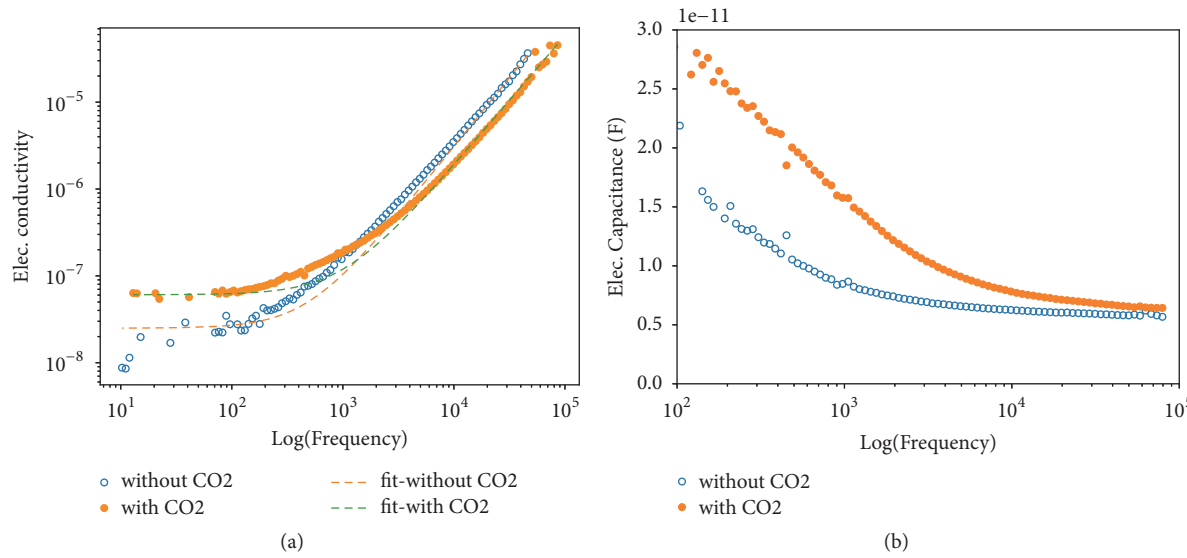

Figure 7: Effect of CO_2 adsorption on the electrical conductivity (a) and electric capacitance (b) of Z5A-1 at 433 K. The dashed lines are fittings with Jonscher's power law.

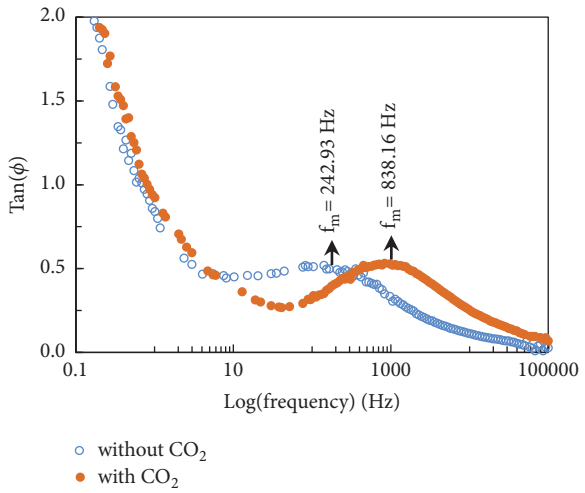

Figure 8: Loss tangent graph versus the logarithm of the frequency of Z5A-1 before and after adsorption of CO_2 at 433 K.

the water vapor pressure in the chamber. It is assumed that the mobility of this sample is caused by the hydroxonium ion H_3O^+ of hydrogen-bonding $H_2O\cdots OH$. Additionally, the hydroxonium concentration also arises from hydroxylation process of Ca^{2+} cations with moderate water as (14). At 373 K, water molecules play a role in supporting proton motion between zeolite lattices via the Grotthuss mechanism [34]. After carbon dioxide is loaded, the concentration of H_3O^+ ions drops immediately because of the weak bonding between $H_2O\cdots OH$. Therefore, the relaxation peak on the modulus M'' and the loss tangent graphs is shifted backward lower frequency after CO_2 loading (Figures 10(a) and 10(b)).

Regarding diffusion process occurring at low frequencies, the impedance can be fitted by finite-length Warburg element as (4). However, due to the influence of gas phase diffusion (i.e., water vapor or CO_2), the impedance spectra have the shape of a semicircle which is represented by a parallel R-CPE. Before CO_2 adsorption, this semicircle is attributed to the water vapor diffusion in high voltage condition. The characterization is still right in case CO_2 is loaded. The presence of CO_2 does not give identification for its diffusivity; carbon dioxide in this case just impacts the diffusivity of water vapor and ionic mobility.

Two diffusion coefficients ($\mathbf{D_m}$, $\widetilde{\mathbf{D}}$) exhibited in Table 5 are diffusion coefficient of ionic mobility H_3O^+ ions and the self-diffusion coefficient of water vapor in zeolite, respectively. Both decrease slightly after CO_2 loading. In comparison, diffusion coefficient of proton mobility was reported in range of (2.5 – 5.0) $x10^{-6}\,cm^2/s$ at 373 K in hydrated zeolite NaY [40] and $7\ x10^{-5}\,cm^2/s$ at room temperature in Nafion/ZrO_2-SO_4^{2-} [41]. Meanwhile, the diffusion coefficient of water vapor was also given as $4.7\ x10^{-5}\,cm^2/s$ at 363 K [41]. Although the estimated values differ slightly compared with results in literature due to some conditions, they are in the same order of magnitude. The mechanism of hydroxonium

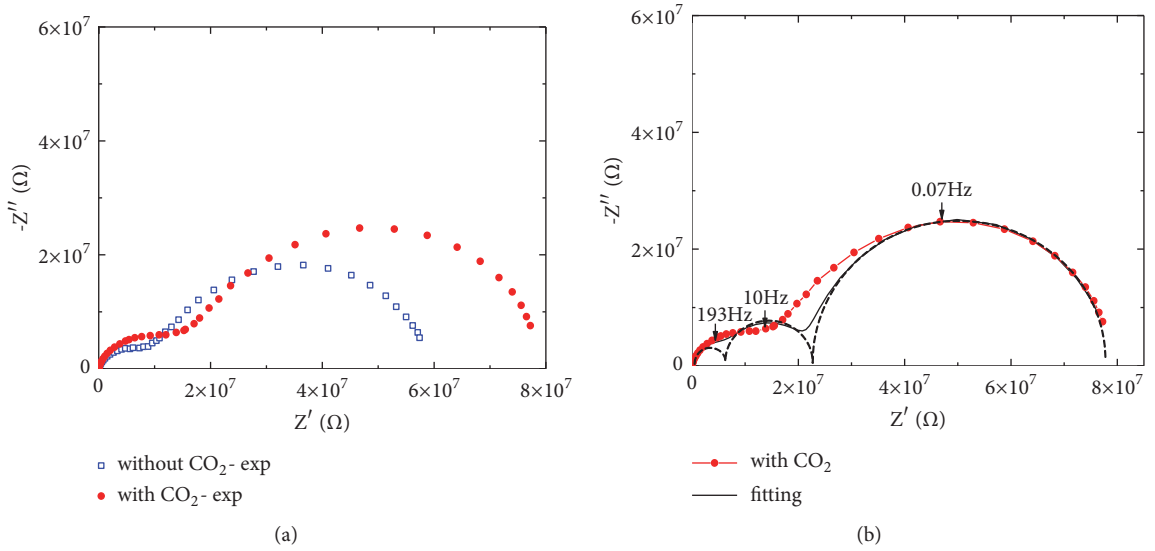

Figure 9: (a) Impedance of Z5A-2 at 373 K with/without CO_2; (b) curve fitting by an equivalent circuit.

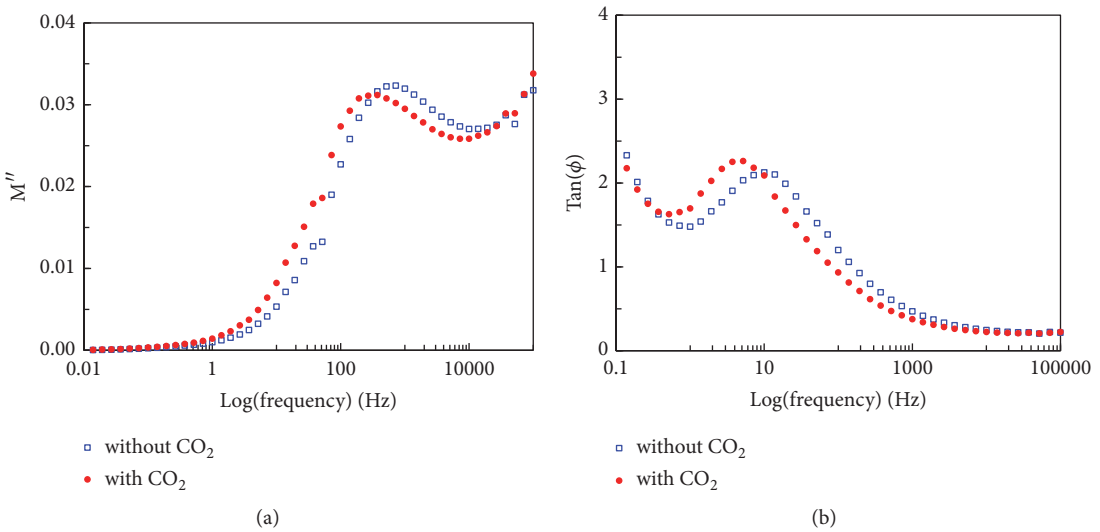

Figure 10: (a) Modulus loss M'' and (b) loss tangent graphs with and without CO_2 of Z5A-2 at 373 K.

ions transfer can be assumed via the Grotthuss mechanism and/or vehicle mechanism [34] under the effect of temperatures and the electric force. Water molecules play a part in promoting and supporting hydroxonium ions transfer between two sites. After carbon dioxide is introduced into the closed chamber, the gradient of the bulk gas influences the removal of a few water molecules on the chain, which encourages hydroxonium ions transfer between two sites. It can interact with weak hydrogen bonded H_3O^+-ion on the surface to generate water molecules. Consequently, three diffusion coefficients in Tables 5 and 6 become a little bit smaller after carbon dioxide flows into the chamber. In comparison with sample Z5A-1, the diffusion coefficient of proton increases after the presence of CO_2. The difference is caused by the strong bond of proton on acid sites; carbon dioxide only helps to enhance the relaxation but cannot remove protons out of the surface.

5. Conclusion

The new proposed approach was effectively applied to compute transport coefficients of gas adsorption in porous solids derived from EIS data. Four transport coefficients can be defined by this method. In case of ammonia adsorption, the mobility diffusion coefficient depends on the concentration of ammonium ions at the interface, which results in an increase of the electrical conductivity. The diffusion coefficient of ammonia in sulfated zirconia is estimated to be approximately the mobility diffusion coefficient of ammonium ions. In the event of carbon dioxide adsorption,

Table 6: Effective diffusion coefficients for sample Z5A-2 at 373 K, p = 1.5 bar.

		Before	After
Binary diffusion coefficient	[cm^2/s]	0.330 ($D_{H2O/air}$)	0.157 ($D_{H2O/CO2}$)
Pressure	[bar]	1	1.5
Stagnant gas layer, l_{st}	[cm]	0.838	0.785
D_e	**[cm^2/s]**	**0.319**	**0.154**

proton and hydroxonium ions in two types of samples are charged carriers. The diffusion coefficient of carbon dioxide cannot be directly calculated from the impedance data. It can be only evaluated by its effect on diffusion coefficient of proton mobility, the self-diffusion coefficient of water vapor in the zeolite pellet, and the effective diffusion coefficient above electrodes.

Data Availability

The data used to support the findings of this study are available from the corresponding author upon request.

Conflicts of Interest

The authors declare that they have no conflicts of interest.

Acknowledgments

The authors thankfully acknowledge the financial support provided by DAAD (A/10/75442), Graduate Academy-Technical University of Dresden, and The Ministry of Education and Training (MoET), Vietnam.

References

[1] W. G. Bessler, "A new computational approach for SOFC impedance from detailed electrochemical reaction-diffusion models," *Solid State Ionics*, vol. 176, no. 11-12, pp. 997–1011, 2005.

[2] Y. Cheng, Q. Huang, M. Eić, and B. J. Balcom, "CO_2 dynamic adsorption/desorption on zeolite 5A studied by 13C magnetic resonance imaging," *Langmuir*, vol. 21, no. 10, pp. 4376–4381, 2005.

[3] S. Primdahl and M. Mogensen, "Gas diffusion impedance in characterization of solid oxide fuel cell anodes," *Journal of The Electrochemical Society*, vol. 146, no. 8, pp. 2827–2833, 1999.

[4] G. Hagen, A. Dubbe, G. Fischerauer, and R. Moos, "Thick-film impedance based hydrocarbon detection based on chromium(III) oxide/zeolite interfaces," *Sensors and Actuators B: Chemical*, vol. 118, no. 1-2, pp. 73–77, 2006.

[5] M. E. Franke and U. Simon, "Solvate-supported proton transport in zeolites," *ChemPhysChem*, vol. 5, no. 4, pp. 465–472, 2004.

[6] U. Simon, U. Flesch, W. Maunz, R. Müller, and C. Plog, "The effect of NH3 on the ionic conductivity of dehydrated zeolites Na beta and H beta," *Microporous and Mesoporous Materials*, vol. 21, no. 1–3, pp. 111–116, 1998.

[7] S. Hara and M. Miyayama, "Proton conductivity of superacidic sulfated zirconia," *Solid State Ionics*, vol. 168, no. 1-2, pp. 111–116, 2004.

[8] D. M. Ruthven, "Diffusion in type A zeolites: New insights from old data," *Microporous and Mesoporous Materials*, vol. 162, pp. 69–79, 2012.

[9] H. Ahn, J.-H. Moon, S.-H. Hyun, and C.-H. Lee, "Diffusion mechanism of carbon dioxide in zeolite 4A and CaX pellets," *Adsorption*, vol. 10, no. 2, pp. 111–128, 2004.

[10] A. Satsuma, K.-I. Shimizu, K. Kashiwagi et al., "Ammonia sensing mechanism of tungstated-zirconia thick film sensor," *The Journal of Physical Chemistry C*, vol. 111, no. 32, pp. 12080–12085, 2007.

[11] S. Matysik, K.-D. Schulze, and C. Breitkopf, "Impedance spectroscopy on solid sulfated zirconia catalysts," *Computer and Experimental Simulations in Engineering and Science*, no. 4, pp. 25–31, 2009.

[12] H. Nakajima, T. Kitahara, and T. Konomi, "Electrochemical impedance spectroscopy analysis of an anode-supported microtubular solid oxide fuel cell," *Journal of The Electrochemical Society*, vol. 157, no. 11, pp. B1686–B1692, 2010.

[13] S. Kouva, J. Kanervo, F. Schüßler, R. Olindo, J. A. Lercher, and O. Krause, "Sorption and diffusion parameters from vacuum-TPD of ammonia on H-ZSM-5," *Chemical Engineering Science*, vol. 89, pp. 40–48, 2013.

[14] R. Staudt, H. Rave, and J. U. Keller, "Impedance spectroscopic measurements of pure gas adsorption equilibria on zeolites," *Adsorption*, vol. 5, no. 2, pp. 159–167, 1999.

[15] F. Jaouen, G. Lindbergh, and K. Wiezell, "Transient techniques for investigating mass-transport limitations in gas diffusion electrodes. II. Experimental characterization of the PEFC cathode," *Journal of The Electrochemical Society*, vol. 150, no. 12, pp. A1711–A1717, 2003.

[16] M. M. Abdel-Gawad and S. V. Bhat, "Evaluation of diffusion coefficient and ionic mobility in $(NH_4)_4Fe(CN)_6x1.5\ H_2O$," *Solid State Ionics*, vol. 28-30, no. 1, pp. 647–650, 1988.

[17] O. Geier, S. Vasenkov, D. Freude, and J. Kärger, "PFG NMR observation of an extremely strong dependence of the ammonia self-diffusivity on its loading in H-ZSM-5," *Journal of Catalysis*, vol. 213, no. 2, pp. 321–323, 2003.

[18] H. Jobic, H. Ernst, W. Heink, J. Kärger, A. Tuel, and M. Bée, "Diffusion of ammonia in silicalite studied by QENS and PFG NMR," *Microporous and Mesoporous Materials*, vol. 26, no. 1-3, pp. 67–75, 1998.

[19] M. S. Whittingham, P. S. Connell, and R. A. Huggins, "An NMR study of ionic motion in ammonium ferrocyanide," *Journal of Solid State Chemistry*, vol. 5, no. 2, pp. 321–327, 1972.

[20] T. Montanari and G. Busca, "On the mechanism of adsorption and separation of CO_2 on LTA zeolites: An IR investigation," *Vibrational Spectroscopy*, vol. 46, no. 1, pp. 45–51, 2008.

[21] D. Amari, J. M. Lopez Cuesta, N. P. Nguyen, R. Jerrentrup, and J. L. Ginoux, "Chemisorption and physisorption of CO_2 on cation exchanged zeolites A, X and mor," *Journal of Thermal Analysis and Calorimetry*, vol. 38, no. 4, pp. 1005–1015, 1992.

[22] G. Onyestyák, D. Shen, and L. V. C. Rees, "Frequency-response studies of CO2 diffusion in commercial 5A powders and pellets," *Microporous Materials*, vol. 5, no. 5, pp. 279–288, 1996.

[23] Y. H. Ma and C. Mancel, "Diffusion stidies of CO_2, NO, NO_2 , and SO_2 on molecular sieve Zeolites by gas Chromatography," *AIChE Journal*, vol. 18, no. 6, pp. 1148–1153, 1972.

[24] E. Barsoukov and J. R. Macdonald, *Impedance Spectroscopy: Theory, Experiment, and Applications*, John Wiley & Sons, 2005.

[25] T. M. W. J. Bandara and B.-E. Mellander, "Evaluation of mobility, diffusion coefficient and density of charge carriers in ionic liquids and novel electrolytes based on a new model for dielectric response," in *Ionic Liquids: Theory, Properties, New Approaches*, InTech, 2011.

[26] P. Demontis, H. Jobic, M. A. Gonzalez, and G. B. Suffritti, "Diffusion of water in zeolites naX and naY studied by quasi-Elastic neutron scattering and computer simulation," *The Journal of Physical Chemistry C*, vol. 113, no. 28, pp. 12373–12379, 2009.

[27] J. Kärger, H. Pfeifer, F. Stallmach, N. N. Feoktistova, and S. P. Zhdanov, "129Xe and 13C PFG n.m.r. study of the intracrystalline self-diffusion of Xe, CO2, and CO," *Zeolites*, vol. 13, no. 1, pp. 50–55, 1993.

[28] R. Coelho, *Physics of Dielectrics—for the Engineer*, vol. 1 of *Fundamental Studies in Engineering*, Elsevier, Amsterdam, The Netherlands, 1979.

[29] J. Bisquert, F. Fabregat-Santiago, I. Mora-Sero, G. Garcia-Belmonte, and S. Giménez, "Electron lifetime in dye-sensitized solar cells: theory and interpretation of measurements," *The Journal of Physical Chemistry C*, vol. 113, no. 40, pp. 17278–17290, 2009.

[30] B. Roling, C. Martiny, and K. Funke, "Information on the absolute length scales of ion transport processes in glasses from electrical conductivity and tracer diffusion data," *Journal of Non-Crystalline Solids*, vol. 249, no. 2-3, pp. 201–209, 1999.

[31] J. R. Dygas, "Dielectric function of ionic conductors studied by impedance spectroscopy," *Solid State Ionics*, vol. 176, no. 25-28, pp. 2065–2078, 2005.

[32] S. P. Jiang and S. P. S. Badwal, "An electrode kinetics study of H_2 oxidation on $Ni/Y_2O_3/ZrO_2$ cermet electrode of the solid oxide fuel cell," *Solid State Ionics*, vol. 123, no. 1-4, pp. 209–224, 1999.

[33] W. Schelder, "Theory of the frequency dispersion of electrode polarization. Topology of networks with fractional power frequency dependence," *The Journal of Physical Chemistry C*, vol. 79, no. 2, pp. 127–136, 1975.

[34] P. Chen, S. Schönebaum, T. Simons et al., "Correlating the integral sensing properties of zeolites with molecular processes by combining broadband impedance and drift spectroscopy—a new approach for bridging the scales," *Sensors*, vol. 15, no. 11, pp. 28915–28941, 2015.

[35] P. Bruce, M. John, and P. John, *The Properties of Gases and Liquids*, vol. 5, Mcgraw-hill, New York, NY, USA, 2009.

[36] P. Demontis, J. Gulín-González, H. Jobic, and G. B. Suffritti, "Diffusion of Water in Zeolites Na A and NaCa A: A Molecular Dynamics Simulation Study," *The Journal of Physical Chemistry C*, vol. 114, no. 43, pp. 18612–18621, 2010.

[37] P. Kurzweil, W. Maunz, and C. Plog, "Impedance of zeolite-based gas sensors," *Sensors and Actuators B: Chemical*, vol. 25, no. 1–3, pp. 653–656, 1995.

[38] G. M. Pajonk, S. J. Teichner, and J. E. Germain, *Spillover of Adsorbed Species: Proceedings of The International Symposium*, vol. 17, Lyon-Villeurbanne: Elsevier, 1983.

[39] J. J. Fripiat, *Proton and Oxygen Mobility in Near-Faujasite Zeolites*, vol. 5, Elsevier Scientific Publishing Company, 1980.

[40] D. Freude, S. Beckert, F. Stallmach et al., "Ion and water mobility in hydrated Li-LSX zeolite studied by 1H, 6Li and 7Li NMR spectroscopy and diffusometry," *Microporous and Mesoporous Materials*, vol. 172, pp. 174–181, 2013.

[41] P. Choi, N. H. Jalani, and R. Datta, "Thermodynamics and proton transport in Nafion III. Proton transport in Nafion/sulfated ZrO2 nanocomposite membranes," *Journal of The Electrochemical Society*, vol. 152, no. 8, pp. A1548–A1554, 2005.